Journal of the Korean Physical Society (2022) 81:935–941
https://doi.org/10.1007/s40042-022-00649-x

Online ISSN 1976-8524
Print ISSN 0374-4884

ORIGINAL PAPER - ATOMS, MOLECULES AND OPTICS

Design of Ag–Ga–$S_{2-x}Se_x$-based eco-friendly core/shell quantum dots for narrow full-width at half-maximum using noble $ZnGa_2S_4$ shell material

Seung-Jae Lee[1] · Ji-Eun Lee[2] · Chang-Jin Lee[1] · Ui-Hyun Jeong[1] · Woo-Guk Lee[3] · Hyo-Jun Kwon[1] · Min-Won Kim[1] · Tae-Hun Shim[1] · Jea-Gun Park[1,3]

Received: 29 September 2022 / Revised: 11 October 2022 / Accepted: 13 October 2022 / Published online: 26 October 2022

Abstract

I–III–VI-based quantum dots (QDs) are promising eco-friendly light-emitting materials for next-generation displays. Thus far, I–III–VI-based QDs (i.e., $AgIn_{1-x}Ga_xS_2$) are still insufficient as light-emitting materials for display fields because of their deteriorated optical properties caused by lattice mismatch between the core/shell materials. We designed a novel passivation process using a shell material (i.e., $ZnGa_2S_4$) with crystalline structure identical to that of $AgGaS_{2-x}Se_x$ core QDs (tetragonal). Green and red light-emitting $AgGaS_2/ZnGa_2S_4$ core/shell QDs demonstrated superior optical properties owing to the minimum lattice mismatch between the $AgGaS_{2-x}Se_2$ core and $ZnGa_2S_4$ shell materials. In particular, a higher quantum yield (QY) and narrow full-width at half-maximum (FWHM) for the green and red light-emitting QDs were achieved, i.e., QYs of 69% and 64% and FWHMs of 26 and 28 nm, respectively. In addition, this remarkable enhancement of optical properties resulted in an increase of ~ 94.4% in the color-space agreement with ITU-R recommendation BT.2020. This means that $AgGaS_{2-x}Se_x$-based core/shell QDs have the potential to be used as eco-friendly QDs for light-emitting materials in next-generation displays.

Keywords $AgGaS_{2-x}Se_x$-based QD · FWHM · PL · Crystalline structure · Color gamut · BT 2020

1 Introduction

Quantum dots (QDs) have been researched intensively for several luminescent materials because of the adjustability of their properties, including wavelength, efficiency (i.e., high QY), stability, and color purity (i.e., narrow FWHM). For this reason, many studies have been conducted on the photovoltaic, detector, bio-imaging, and display fields in recent decades [1–4]. In particular, light-emitting materials for display applications (i.e., QD-OLED and QLED) were found to require more than 95% QY and less than 30 nm narrow FWHM [5–7]. For instance, cadmium (Cd)-based QDs (CdSe QDs) of the II–VI materials have superior optical properties with high QY (over 95%), high stability, and narrow FWHM (> 25 nm). However, due to environmental issues, the use of Cd has been restricted in display applications according to the European Restriction of Hazardous Substances (RoHS) specification [8–11]. By contrast, light-emitting materials for display applications based on indium phosphide (InP) of III–V materials comply with RoHS standards. In particular, the InP-based QD of a III–V material structure (bulk bandgap energy of ~ 1.35 eV) can control the energy from near blue (~ 2.5 eV) to near infrared (~ 1.7 eV) by adjusting the core size [12–15]. Although eco-friendly InP-based QDs have been actively studied, they have limitations in improving the narrow FWHM (less than 30 nm) because of their large lattice covalency (the electrons shared with other atoms), resulting in the broad FWHM characteristics of InP-based QDs [16–18]. In general, the lattice covalency can be characterized using Phillips ionicity, which represents a quantified value for the type of chemical bonds between ionic (larger Phillips ionicity) and covalent

✉ Jea-Gun Park
parkjgl@hanyang.ac.kr

[1] Department of Electronic Engineering, Hanyang University, Seoul 04763, Republic of Korea

[2] Department of Information Display Engineering, Hanyang University, Seoul 04763, Republic of Korea

[3] Department of Nanoscale Semiconductor Engineering, Hanyang University, Seoul 04763, Republic of Korea

bonding (smaller Phillips ionicity) [19–21]. Note that the Phillips ionicity of InP-based QDs is small because of the covalent bonding between In^{3+} and P^{3-} atoms, and thus they have a relatively larger lattice covalency compared to CdSe-based QDs (Phillips ionicities of InP and CdSe are 0.421 and 0.699, respectively) [17, 19]. Accordingly, the larger lattice covalency of InP-based QDs intrinsically requires a high growth temperature (~300 °C) and reactive precursors (Tris(trimethylsilyl) phosphide). Therefore, InP-based QDs have the optical properties of broad particle size distribution (broad FWHM), because they require high energy for the nucleation and growth steps of the InP core QDs [22–24]. Thus far, it has been reported that $AgIn_xGa_{1-x}S_2$ ($AgIn_xGa_{1-x}S_2/Ga_2S_3$)-based core/shell QDs of I–III–V core materials have high Phillips ionicities (~0.813) [19, 25]. However, the core/shell QDs of $AgIn_xGa_{1-x}S_2/Ga_2S_3$ are difficult to passivate perfectly with a shell material because of the lattice mismatch (~8.5%) of crystalline structures between the $AgIn_xGa_{1-x}S_2$ core (tetragonal) and Ga_2S_3 shell (hexagonal), resulting in poor optical properties of QY (less than 50%) and wider FWHM (wider than 40 nm) [26–30].

In this study, $AgGaS_{2-x}Se_x$-based core QDs as light-emitting materials with ionic bonds of larger phillip ionicity (~0.729) were designed for green and red light-emitting core QDs. In addition, shell structures (Ga_2S_3, $ZnGa_2S_4$, and ZnS) were introduced to achieve the optical properties of high QY and narrow FWHM of the $AgGaS_{2-x}Se_x$-based core/shell QDs, as shown in Fig. 1. Furthermore, we conducted a novel synthesis of I–III–VI-based core/shell QDs with a very narrow FWHM characteristic (less 30 nm) through passivation using a shell material ($ZnGa_2S_4$) with a crystalline structure identical to that of $AgGaS_{2-x}Se_x$ core QDs (tetragonal) to minimize lattice mismatch (~6.5%) between core/shell materials. In particular, the optical properties, crystallinities, and morphologies of the three types of shell structures on the $AgGaS_{1-x}Se_x$-based core QDs were investigated to enhance the color-space matching with the BT 2020 standard by improving the emission wavelength and FWHM.

2 Experiments and discussion

2.1 Materials

Oleylamine (OAm, 70%), 1-dodecanethiol (DDT, > 98%), silver acetate (Ag(OAc), 99.99%), gallium(III) acetylacetonate ($Ga(acac)_3$, 99.99%), tetramethylthiuram disulfide (TMTDS, 97%), zinc acetate ($Zn(OAc)_2$, 99.99%), trioctylphosphine (TOP, 97%), selenium (trace metals basis, 100 mesh, and 99.99%), and oleic acid (OA, technical grade 90%) supplied by Sigma-Aldrich were used.

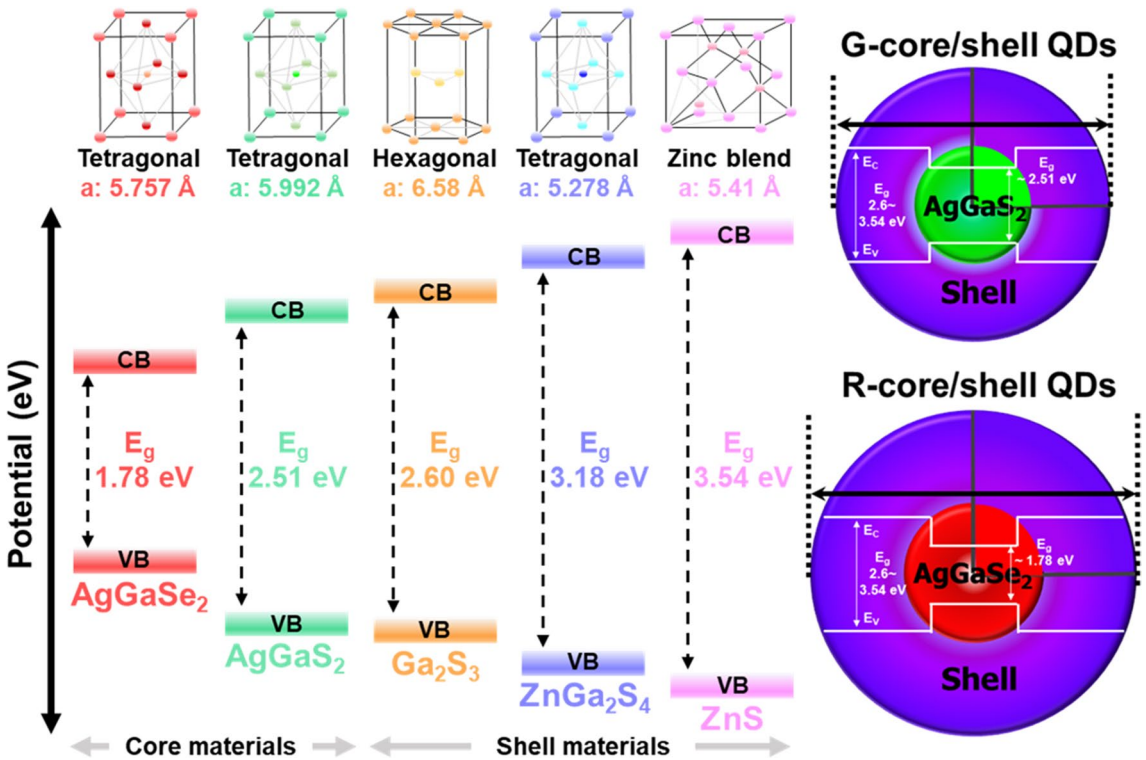

Fig. 1 Crystalline structure and energy bandgap diagram according to core/shell QDs. The schematic of a core/shell QD structure depending on the core materials (right images)

2.2 Preparation of precursors

Ag (OAc)-Oam (0.5 M) was prepared by dissolving 1 mmol of Ag(Oac) powder in 2 ml of OAm in an N_2-filled glove box. A 0.5 M TMTDS-OAm precursor was prepared with 1 mmol of TMTDS dissolved in 2 ml of OAm in an N_2-filled glove box. A 0.5 M Se-OAm precursor was prepared with 1 mmol of Se powder dissolved in 2 ml of OAm in an N_2-filled glove box. Then, all the precursors were evacuated at 150 °C for 1 h and heated to 170 °C under N_2 flow. A 0.5 M $Ga(acac)_3$-ODE precursor was prepared with 1 mmol of $Ga(acac)_3$ dissolved in 2 ml of ODE in an N_2-filled glove box. A 1 M $Zn(oleate)_2$ precursor was prepared by dissolving 5 mmol of $Zn(OAc)_2$ in 10 ml of ODE and oleic acid, and the precursors were evacuated at 150 °C for 1 h and heated to 250 °C under N_2 flow.

2.3 Synthesis of green and red light-emitting $AgGaS_2$ and $AgGaSe_2$ core/shell QDs

For the $AgGaS_2$ and $AgGaSe_2$ for green and red light-emitting cores, 0.5 mmol of Ag(OAc) and $Ga(acac)_3$ each were loaded into a 100 mL three-neck flask with 14 mL OAm at room temperature. The mixture was heated to 150 °C while being stirred, and then degassed under a pressure of 100 mTorr for 1 sh. Then, the precursor solution for 0.6 mL of 0.5 M TMTDS-OAm (green-light emitting core QDs) or 0.4 mL Se-OAm (red light-emitting core QDs) was rapidly injected in the mixture at 200 or 220 °C for 40 min under N_2 flow. For $ZnGa_2S_4$ shell growth, 7.6 mL of $Zn(oleate)_2$, $Ga(acac)_3$, DDT, and ODE precursors were slowly added dropwise into the core mixture at 240 °C for 90 min. After the $ZnGa_2S_4$ shell growth, the solution was cooled to room temperature and then centrifuged with an excessive amount of acetone (at least 3 times) to eliminate the impurities of unreacted starting materials and side products. Finally, the precipitated QDs were redispersed in 5 mL of an organic solvent. The detailed morphology, crystallinity, crystalline structure, size distribution, and core/shell structures of the $AgGaS_{1-x}Se_x$-based core/shell QDs were characterized by transmission electron microscopy (TEM) at an acceleration voltage of 200 kV, energy-dispersive X-ray spectroscopy (EDX), and X-ray diffraction (XRD). The optical properties were measured by UV–visible absorption spectra using a Carry-5000 (Varian), and the photoluminescence (PL) spectra were measured using a HeCd laser source at an 325 nm excitation wavelength. The FWHM and absolute PL QY were measured using a QE-2100 (Otsuka Electronics).

3 Results and discussion

To estimate the optical properties depending on the crystalline structures of the shell materials, three types of shell materials (Ga_2S_3, $ZnGa_2S_4$, and ZnS) on $AgGaS_{1-x}Se_x$ core QDs were designed, as shown in Fig. 1. In general, the lattice mismatch between the core and shell induces strain at their interface, leading to deteriorating optical properties. Thus, to improve the optical properties, it is necessary to apply an identical crystalline structure of the core with shell materials, for a minimum lattice mismatch between the core and shell, and wider bandgap energy of the shell materials than of the core material.

As shown in Fig. 2, it was confirmed that the optical properties (emitting wavelength, QY, and FWHM) depend on the shell bandgap energy and crystalline structures on the core, i.e., bulk bandgap energies of the $AgGaSe_2$, $AgGaS_2$, Ga_2S_3, $ZnGa_2S_4$, and ZnS materials were 1.78, 2.51, 2.60, 3.18, and 3.54 eV, respectively. The absorption and emission spectra of the G-$AgGaS_2$- and R-$AgGaSe_2$-based core/shell QD are presented in Fig. 2a, b, respectively. The absorption and PL spectra of the three types of shells passivated on the G-$AgGaS_2$- and R-$AgGaSe_2$-core QDs were obviously different. Accordingly, in the case of G-$AgGaS_2$-based core/shell QDs, the absorption spectra increased from the UV to the visible light region (300,550 nm) when passivated by shell materials (Ga_2S_3, $ZnGa_2S_4$, and ZnS). As a result, the QYs of three types of G-$AgGaS_2$-based core/shell QDs were 22%, 69%, and 52%, respectively, which translated to ~ 2.4, 7.6, and 5.7 times higher than those for the G-$AgGaS_2$ core

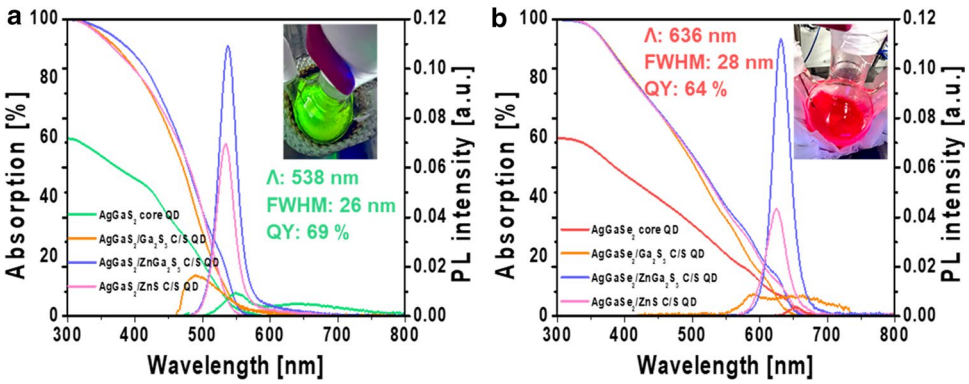

Fig. 2 Absorption and PL spectra of the green light-emitting $AgGaS_2$-based core/shell QDs and the **a** red light-emitting $AgGaSe_2$-based core/shell QDs, **b** depending on the shell structures excited under 450 nm. Photographs (insets in **a** and **b**) of solution-based QDs under 365 nm hand-UV lamp for G-$AgGaS_2$/$ZnGa_2S_4$ and R-AgGaSe2/ZnGa2S4 core/shell QDs, respectively

QDs (9%), respectively, as shown in Fig. 2a and Table 1. In addition, the FWHM of the two types ($ZnGa_2S_4$ and ZnS) of G-$AgGaS_2$-based core/shell QDs were 26 and 31 nm, respectively, which translated to ~ 0.62 and 0.74 times narrower than those of the G-$AgGaS_2$ core QDs (42 nm), respectively, because the shell growth of $ZnGa_2S_4$ or ZnS was dominantly reacted rather than diffusion effect of Ga^{3+} and Zn^{2+} ions, as shown in Fig. 2a and Table 1. In the case of shell passivation with Ga_2S_3, the FWHM of the G-$AgGaS_2$/Ga_2S_3 core/shell QDs (55 nm) was wider than that of the G-$AgGaS_2$ core QDs (42 nm), since the diffusion effect of Ga^{3+} ions was mainly reacted rather than Ga_2S_3 shell growth [31]. Thus, the QY and FWHM of the G-$AgGaS_2$/$ZnGa_2S_4$ core/shell QDs with an identical crystalline structure (tetragonal) among three types of shell materials were 69% and 26 nm, respectively, which translated to an enhancement of ~ 7.6 and 0.62 times compared with those for the $AgGaS_2$ core QDs (9% and 42 nm), respectively.

For R-$AgGaSe_2$-based core/shell QDs, the absorption spectra increased from the UV- to visible-light region (300–650 nm) when passivated by shell materials. As a result, the QYs of three types of R-$AgGaS_2$-based core/shell QDs were 19%, 64%, and 46%, respectively, translating to ~ 3.1, 10.6, and 7.6 times higher than those for the R-$AgGaSe_2$ core QDs (6%), respectively, as shown in Fig. 2b and Table 1. In addition, the FWHM of two types ($ZnGa_2S_4$ and ZnS) of R-$AgGaSe_2$-based core/shell QD were 28 and 34 nm, respectively, which translates to ~ 0.75 and 0.91 times narrower than those for the R-$AgGaSr_2$ core QDs (37 nm), as shown in Fig. 2b and Table 1. The FWHM of the R-$AgGaSe_2$/Ga_2S_3 core/shell QDs, in the case of the shell passivated with Ga_2S_3 material, the FWHM of the R-$AgGaSe_2$/Ga_2S_3 core/shell QDs (141 nm) is much wider than that of the R-$AgGaSe_2$ core QDs (37 nm), because not only Ga^{3+} cations but also S^{2-} anion atoms diffuse into the core. Therefore, the Ga_2S_3 shell was unstably passivated on the R-$AgGaSe_2$ core QDs. Therefore, the QY and FWHM of the R-$AgGaSe_2$/$ZnGa_2S_4$ core/shell QDs among three types of shell materials were 64% and 28 nm, respectively, which translates to ~ 10.6 and 0.75 times higher than those for the $AgGaSe_2$ core QDs (6% and 7 nm), respectively. Thus, because the lattice mismatch between the $AgGaS_{x-2}Se_2$ core and $ZnGa_2S_4$ shell (~ 6.5%) was smaller than that of two types of $AgGaS_{x-2}Se_2$/Ga_2S_3 (~ 8.5%) and $AgGaS_{x-2}Se_2$/ZnS (~ 7.7%) core/shell QDs, the optical properties of the $AgGaS_{x-2}Se_2$/$ZnGa_2S_4$ core/shell structure exhibited the best results. Thus, we demonstrate an improvement in the optical properties as a result of the minimal lattice mismatch between the core and shell materials. To confirm this, we discuss it later through XRD and HR-TEM analyses.

To understand why the optical properties of the $ZnGa_2S_4$ shell material were remarkably higher than those of the Ga_2S_3 and ZnS shell materials, the crystallinities of the three types of shell structures were confirmed using selected area diffraction (SAED) and XRD patterns, as shown in Fig. 3a, b. The XRD peak positions of the diffraction peaks ((112), (204), (220), (312), and (224)) of the tetragonal crystalline structure were affected by the differences in the three types of crystalline structures (shell materials). Note that the distinct rings originating from (112), (204), (220), (312), and (224) in the SAED patterns correlated well with the dominant XRD diffraction peaks for the core and three types of core/shell structures. However, in the case of the $AgGaS_{x-2}Se_2$/Ga_2S_3 and $AgGaS_{x-2}Se_2$/ZnS core/shell structures, the XRD peak positions were affected by the crystalline structure of the hexagonal and zinc blends, resulting in a shift in the XRD peak position. The highest crystallinity shown from the relative FWHM of the three types of crystalline structures for the shell materials was observed in the same tetragonal crystalline structure between the core

Table 1 Optical properties of the green and red light-emitting $AgGaS_2$-based core/shell QDs depending on the shell structures

Emitting light color	Core/shell structure	PL λ_{max} [a] [nm]	Abs. λ_{max} [b] [nm]	Stokes shift[c] [nm]	FWHM [nm]	PL-QY[d] [%]
Green light-emitting core/shell QDs	$AgGaS_2$ core	549	531	18	42	9
	$AgGaS_2$/Ga_2S_3 C/S	491	482	9	55	22
	$AgGaS_2$/$ZnGa_2S_4$ C/S	538	515	23	26	69
	$AgGaS_2$/ZnS C/S	534	518	16	31	52
Red light-emitting core/shell QDs	$AgGaSe_2$ core	651	636	15	37	6
	$AgGaSe_2$/Ga_2S_3 C/S	592	586	6	141	19
	$AgGaSe_2$/$ZnGa_2S_4$ C/S	631	615	16	28	64
	$AgGaSe_2$/ZnS C/S	624	610	14	34	46

[a]Wavelength of photoluminescence peak

[b]First peak wavelength of absorption spectra

[c]Difference (in wavelength) between abs. λ_{max} and PL λ_{max}

[d]Measured by absolute PL QY using QE-2100 (Otsuka Electronics)

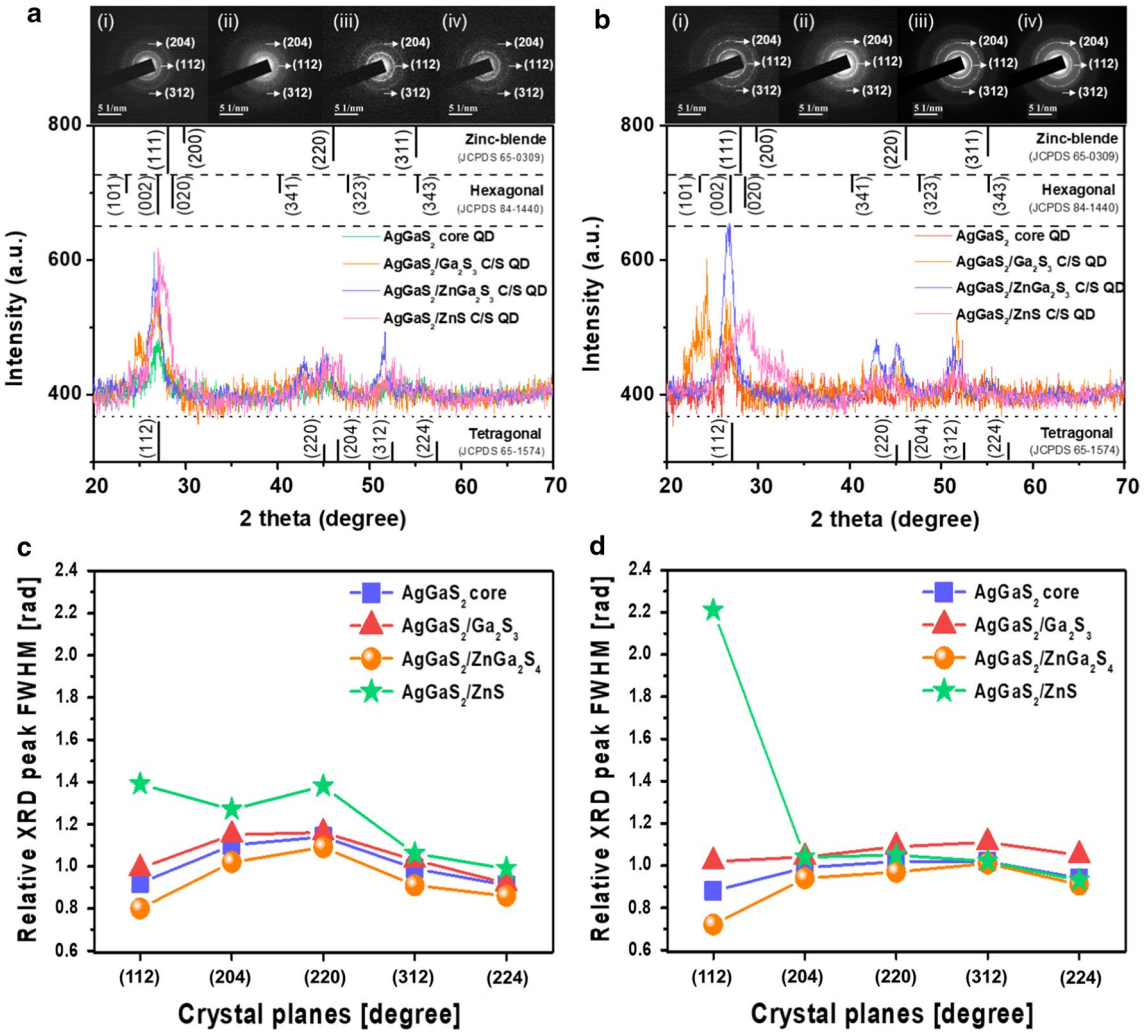

Fig. 3 X-ray diffraction (XRD) patterns of the AgGaS2- **a** and AgGaSe2-based core/shell QDs **b** depending on the shell structures by the Crystalline structure, and corresponding selected area electron diffraction (SAED) patterns (above image). Dependency of the relative XRD peak FWHM for tetragonal crystal planes. The AgGaS2- (**c**) and AgGaSe2-based core/shell QDs **d,** respectively

(G-$AgGaS_2$ and R-$AgGaSe_2$) and shell ($ZnGa_2S_4$) materials. As a result, the relative XRD FWHM at the peak position of the (112) plane of G-$AgGaS_2$/Ga_2S_3 (0.99 rad. a.u.), G-$AgGaS_2$/$ZnGa_2S_4$ (0.8 rad.), and G-$AgGaS_2$/ZnS core/shell QDs (1.39 rad.) were ~ 1.07, 0.87, and 2.1 times wider than that for the $AgGaS_2$ core QDs (0.92 rad.) eV, respectively, as shown in Fig. 3c. For the R-$AgGaSe_2$-based core/shell QDs, the relative XRD FWHM at the peak position of the (112) plane of R-$AgGaS_2$/Ga_2S_3 (1.02 rad.), R-$AgGaSe_2$/$ZnGa_2S_4$ (0.72 rad.) and R-$AgGaS_2$/ZnS core/shell QDs (2.21 rad.) were ~ 1.16, 0.81, and 2.51 times wider than that of the R-$AgGaSe_2$ core QDs (0.88 rad.), respectively, as shown in Fig. 3d. In general, for XRD analysis, the crystallinity showing a narrower FWHM at the XRD peak position is better. Thus, from the results of the XRD analysis, the shell passivation with $ZnGa_2S_4$ material showed the best crystallinity among the three types of shell materials, which resulted in perfect shell passivation on the core QDs.

The spherical-like shape, high crystallinity, good dispersity, and interplanar distance of the core and three types of core/shell structures were compared in detail using HR-TEM images, as shown in Fig. 4. For the G-$AgGaS_2$-based core/shell QDs, when the diameter of the core QDs was 4.1 ± 0.54, the diameters of the core/shell structures passivated with Ga_2S_3, $ZnGa_2S_4$, and ZnS shell materials were 4.4 ± 0.51, 6.8 ± 0.41, and 6.5 ± 0.99 nm, respectively, as shown in Fig. 4a, d. In addition, for the R-$AgGaSe_2$-based core/shell QDs, when the diameter of the core QDs was 6.7 ± 0.84, the diameters of the core QDs and core/shell structures with Ga_2S_3, $ZnGa_2S_4$, and ZnS shell materials were 7.0 ± 0.92, 9.6 ± 0.53, and 8.9 ± 0.92 nm, respectively, as shown in Fig. 4e, h. When the G-$AgGaS_2$ and R-$AgGaSe_2$-based core QDs were passivated with a Ga_2S_3

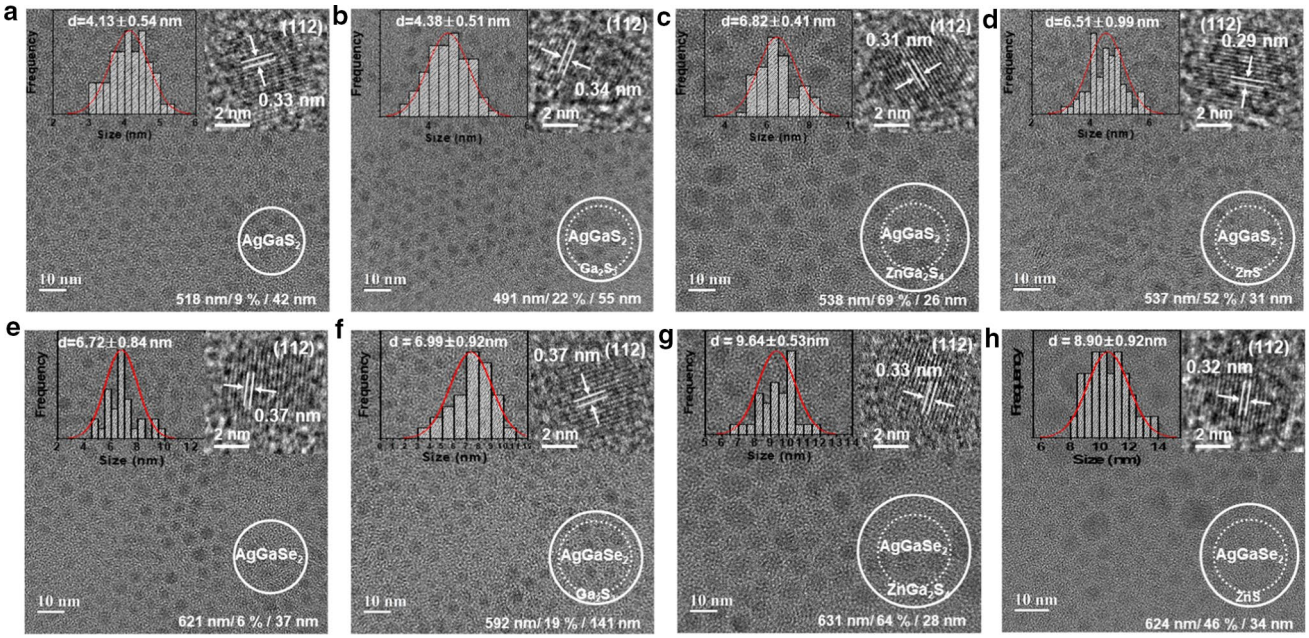

Fig. 4 High-resolution transmission electron microscopy (HRTEM) images of the green **a**–**d** and red light-emitting QDs **e**–**f** depending on the shell structures with a scale bar of 10 nm, size distribution (inset, upper left), and d-spacing values with a scale bar of 2 nm (inset, upper right)

shell material, it was confirmed that the Ga_2S_3 material was not grown as a shell layer and defect sites inside or on the core were passivated with Ga^{3+} ions, as shown in Fig. 4b, f [26, 27]. Furthermore, the interplanar distances of the G-$AgGaS_2$-based core QDs and R-$AgGaSe_2$-based core were 0.33 and 0.37 nm at the (112) plane, as shown in the HR-TEM images of the insets in Fig. 4a, e. Moreover, the interplanar distances of the core/shell structures for the three types of shell materials were altered by the difference in the lattice constant depending on the shell materials. From the XRD patterns and TEM images, it was confirmed that the perfectly spherical shape, thickest shell growth, and narrowest FWHM of G-$AgGaS_2$ (26 nm) and R-$AgGaSe_2$-based core with $ZnGa_2S_4$ shell QDs (28 nm) were attributed to the lattice mismatch of $ZnGa_2S_4$-based core/shell QDs (~6.5%) being the smallest among Ga_2S_3- and ZnS-based core/shell QDs (~8.5% and 7.7%).

Note that the narrow FWHM of the PL spectra of QDs is an important parameter of color purity (color reproducibility) for display characteristics. In addition, QLED–LCD and QD-OLED displays, which use red, green, and blue (RGB) colors transmitted through respective RGB color filters (CFs) from a backlight unit, should comply with the BT 2020 color standard, which is a set of specifications for various aspects of video broadcasting recommended by the ITU as standards for ultra-high-definition (UHD). Therefore, we simulated the agreement with the BT 2020 color standard, according to the FWHM of the G-$AgGaS_2$/$ZnGa_2S_4$ and R-$AgGaSe_2$/$ZnGa_2S_4$ core/shell QDs without CFs at a fixed blue wavelength (455 nm) and FWHM (20 nm), extracted from the green and red light PL spectra, as shown in Fig. 5. A decrease in the FWHM of the green and red light PL spectrum to 20 nm, indicated an improvement of 95.7% with the BT2020 agreement. Finally, in the case of the G-$AgGaS_2$/$ZnGa_2S_4$ and R-$AgGaSe_2$/$ZnGa_2S_4$ core/shell QDs, an improvement of 94.4% with the BT2020 agreement was achieved via optimal optical properties of the green (538 nm of the wavelength and 26 nm of the FWHM) and red light spectra (636 nm of the wavelength and 28 nm of the FWHM), as shown in the enlarged graph of Fig. 5.

4 Conclusions

QDs have been intensively researched as light-emitting materials for display applications because of their adjustable properties, such as the wavelength, efficiency (high QY), stability, and color purity (narrow FWHM of PL spectra). In particular, I–III–VI-based QDs ($AgGaS_{2-x}Se_x$) have attracted interest as promising eco-friendly (cadmium-free) light-emitting materials for next-generation displays. In addition, light-emitting materials for display applications (QD-OLED and QLED) should demonstrate the optical properties of the PL spectra FWHM of less than 30 nm for green and red light-emitting QDs. Although $AgIn_{1-x}Ga_xS_2$-based core/shell QDs (I–III–VI-based QDs) have been reported, they exhibit optical properties with an FWHM of ~40 nm. However, our I–III–VI-based QDs of $AgGaS_{2-x}Se_x$/$ZnGa_2S_4$

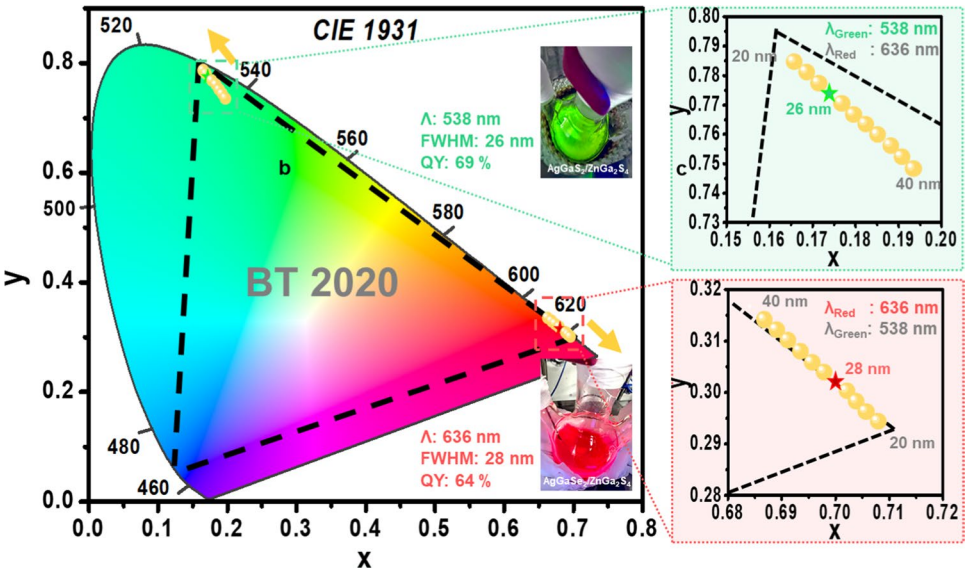

Fig. 5 Shift of coordinates in the color triangle space depending on the FWHM (from 40 to 20 nm) of the emitting spectra for the center peak points at 538 and 636 nm. Enlarged graphs for each region in green (top) and red (bottom) are shown

with a minimum lattice mismatch between the $AgGaS_{2-x}Se_x$ core and $ZnGa_2S_4$ shell and an identical crystal structure (tetragonal) resulted in much narrower FWHMs of the green and red light-emitting QDs (26 and 28 nm). In conclusion, these results indicate that the $AgGaS_{2-x}Se_x/ZnGa_2S_4$ core/shell QDs are nearly comparable to the cadmium-based core/shell QDs (with less than 25 nm of FWHM). In addition, BT 2020 agreement between G-$AgGaS_2/ZnGa_2S_4$ and R-$AgGaSe_2/ZnGa_2S_4$ core/shell QDs was ~ 94.4% without the CFs.

Fundamentally, although $AgIn_{1-x}Ga_xS_2$-based core/shell QDs showed low FWHM (~ 28 nm), the QY of the green and red-light QDs was low (~ 70%), because they were passivated with a monolayer shell structure of $ZnGa_2S_4$. Therefore, further research to achieve a high QY using multi-layered shell structures with the same crystalline structure on $AgIn_{1-x}Ga_xS_2$-based core/shell QDs is necessary.

Acknowledgements This research was supported by a National Research Foundation of Korea (NRF) grant funded by the Korean government (MSIT) (No. 2021R1A4A1052085) and by the Brain Korea 21 PLUS Program.

References

1. Coe-Sullivan et al., ECS J. Solid State Sci. Technol. **2**, 3026–3030 (2013)
2. H. Chen et al., Opt. Express **25**, 102–111 (2017)
3. Luo, Z. et al., 2014 Proc. of SPIE 9005, 90050G1–7
4. M.A. Cotta, ACS Appl. Nano Mater. **3**, 4920–4924 (2020)
5. K.Y. Lai et al., Nanomaterials **12**, 2683 (2022)
6. M.K. Choi et al., npj Flex. Electron. **2**, 1 (2018)
7. J.R. Manders et al., Quantum dots for displays and solid state lighting, in *In Materials for Solid State Lighting and Displays*. ed. by A. Kitai (Wiley Series, Hoboken, 2016), pp.31–90
8. S.A. Kusuma et al., J. Clean. Prod. **366**, 132760 (2022)
9. S. Tsukuda et al., J Soc Inf Disp. **28**, 680–690 (2020)
10. H.S. Moon et al., Adv. Mater. **31**, 157–160 (2019)
11. A. Saha et al., Chem. Mater. **32**, 2148–2155 (2020)
12. D.A. Taylor et al., Chem. Mater. **33**, 4399–4407 (2021)
13. R. Toufanian et al., Front. Chem. **6**, 567–573 (2018)
14. Yi. Zhang et al., Prog. Photovoltaics Res. Appl. **6**, 571–596 (2022)
15. H. Meddeb et al., Adv. Energy Mater. **12**, 2200713 (2022)
16. X. Jiang et al., Micromachines **13**, 709 (2022)
17. E.J. Jang et al., ACS Energy Lett. **5**, 1316–1327 (2020)
18. E.M. Janke, J. Am. Chem. Soc. **140**, 15791–15803 (2018)
19. O.P. Singh et al., Phys. stat. sol. **137**, 97 (1986)
20. K. Hubner et al., Phys. stat. sol. **77**, 473 (1976)
21. J.R. Manders et al., in *Semiconductor Materials: an Introduction to Basic Principles*. ed. by B.G. Yacobi (Springer, Boston, 2003), pp.5–32
22. Y.J. Kwon et al., NPG Asia Mater. **13**, 13–37 (2021)
23. D.C. Gary et al., Chem. Mater. **27**, 1432–1441 (2015)
24. A.L. Efros et al., ACS Nano **15**, 6192–6210 (2021)
25. Y.S. Kim et al., Chem. Sci. **11**, 913–922 (2019)
26. T. Uematsu et al., NPG Asia Mater. **10**, 713–726 (2018)
27. T. Kameyama et al., ACS Appl. Mater. Interfaces **10**, 42844–42855 (2018)
28. W. Hoisang et al., Nanoscale Adv. **4**(2), 849–857 (2022)
29. A. Hirase et al., Phys. Chem. Lett. **11**, 3969–3974 (2020)
30. W. Hoisang et al., Nanomaterials **9**, 1769 (2019)
31. X. Peng et al., J. Am. Chem. Soc. **119**, 7019–7028 (1997)